ORIGINAL PAPER

Atmospheric processes responsible for generation of the 2008 Boothbay meteotsunami

I. Vilibić · K. Horvath · N. Strelec Mahović · S. Monserrat ·
M. Marcos · Á. Amores · I. Fine

Abstract   We investigated the atmospheric processes and physics that were active during a tsunami-like event hitting Boothbay Harbor area (Maine, USA) on 28 October 2008. The data collected by tide gauges, ground and sounding stations and meteo–ocean buoys in the area were analyzed, together with satellite and radar images. The atmospheric processes were reproduced by the weather research and forecasting model, verified by in situ and remote sensing data. A cold front moved over the area at the time of the event, with embedded convective clouds detected by satellite and radar data and the internal gravity waves (IGWs) detected by radar and reproduced by the model at the rear of the frontal precipitation band. According to the model, the IGWs that passed over Boothbay Harbor generated strong ground air-pressure oscillations reaching 2.5 hPa/3 min. The IGWs were ducted towards the coast without significant dissipation, propagating in a stable near-surface layer capped by an instability at approximately 3.5 km height and satisfying all conditions for their maintenance over larger areas. The intensity, speed and direction of the IGWs were favourable for generation of a meteotsunami wave along the Gulf of Maine shelf. Operational observation systems were not capable of sufficiently capturing the ground disturbance due to a too coarse sampling rate, while the numerical model was found to be a useful tool in eventual future detection and warning systems.

I. Vilibić (✉)
Institute of Oceanography and Fisheries, Šetalište I. Meštrovića 63, 21000 Split, Croatia
e-mail: vilibic@izor.hr

K. Horvath · N. Strelec Mahović
Meteorological and Hydrological Service, Grič 3, 10000 Zagreb, Croatia

S. Monserrat · M. Marcos · Á. Amores
IMEDEA (CSIC-UIB), Ctra. Valldemossa, km. 7.5, Palma de Mallorca, Spain

I. Fine
Fisheries and Oceans Canada, Ocean Science Division, Institute of Ocean Sciences,
9860 W. Saanich Rd., Sidney, BC, Canada

1 Introduction

On 28 October 2008 at 19 UTC, giant waves hit the coasts of Maine, with the highest one occurring at Boothbay Harbor (Fig. 1). Eyewitnesses reported the height at approximately 4 m and the wave period of about 20 min, fortunately occurring during a low tide. Strong currents and whirlpools were observed as well. No earthquakes capable of generating such waves were reported at the time. Likewise, almost 400-km-wide shelf off the coast of Maine and the spatial limit of the observed event exclude a submarine landslide as a potential generator of the event. Atmospheric processes are left as a likely source of the event. Similar events have been occasionally documented along the U.S. East Coast (Nikolkina and Didenkulova 2012) and associated with propagating atmospheric pressure disturbances (Churchill et al. 1995; Sallenger et al. 1995; Paxton and Sobien 1998) or storms (Mercer et al. 2002; Thomson et al. 2007; Yankovsky 2009), which can resonantly excite long ocean waves through open-ocean and topographical resonances over a wide shelf area.

This phenomenon is called a meteorological tsunami or meteotsunami (Monserrat et al. 2006) and is found to occur in oceans worldwide (Hibiya and Kajiura 1982; Monserrat et al. 1991; Mecking et al. 2000; Dragani et al. 2002; Vilibić and Šepić 2009; Haslett and Bryant 2009). The strength of a meteotsunami is usually proportional to the rate of change of air pressure over the span of several minutes (Šepić and Vilibić 2011) and to the efficiency of the resonant energy transfer to the ocean which is dependent on ratio between the speed of the atmospheric pressure disturbance and speed of long ocean waves, with the latter determined by bathymetry (Vilibić 2008), and some other factors (in particular wave direction). Hibiya and Kajiura (1982) derived a simplified formula for sea-level resonant amplification of the ocean waves under fully resonant conditions, $\eta(t) = \eta_0 Ut/2\lambda$, where U is the disturbance speed, η_0 inverse barometer factor, λ the distance on which the pressure gradient linearly increases and t the time. The formula simply states that shorter disturbances may transfer energy to the sea over shorter distances and in shorter time span. Aside from the resonant energy transfer from the atmosphere to the sea, strong coastal amplification is necessary for a meteotsunami to reach destructive levels, consequently restricting these several metre high sea-level oscillations to elongated inlets, bays and harbours which have strong amplification factors (Rabinovich 2009; Orlić et al. 2010).

Normally, the generator of a meteotsunami is a travelling atmospheric disturbance (Monserrat et al. 2006) restricted and transmitted to the lower troposphere and therefore visible in surface air-pressure series; however, wind variability can contribute to meteotsunami generation as well (de Jong and Battjes 2004). The disturbance, which can be in form of a pressure jump, atmospheric gravity wave, or a squall line, can maintain its intensity over long distances under specific atmospheric conditions, mainly related to wave-duct or wave-CISK mechanisms. Wave-duct mechanism occurs when a stable lower troposphere with an increasing wind in a vertical direction is overtopped with an unstable layer in mid-troposphere, reflecting the energy towards the surface and ducting gravity waves over long distances (Lindzen and Tung 1976; Monserrat and Thorpe 1996). The
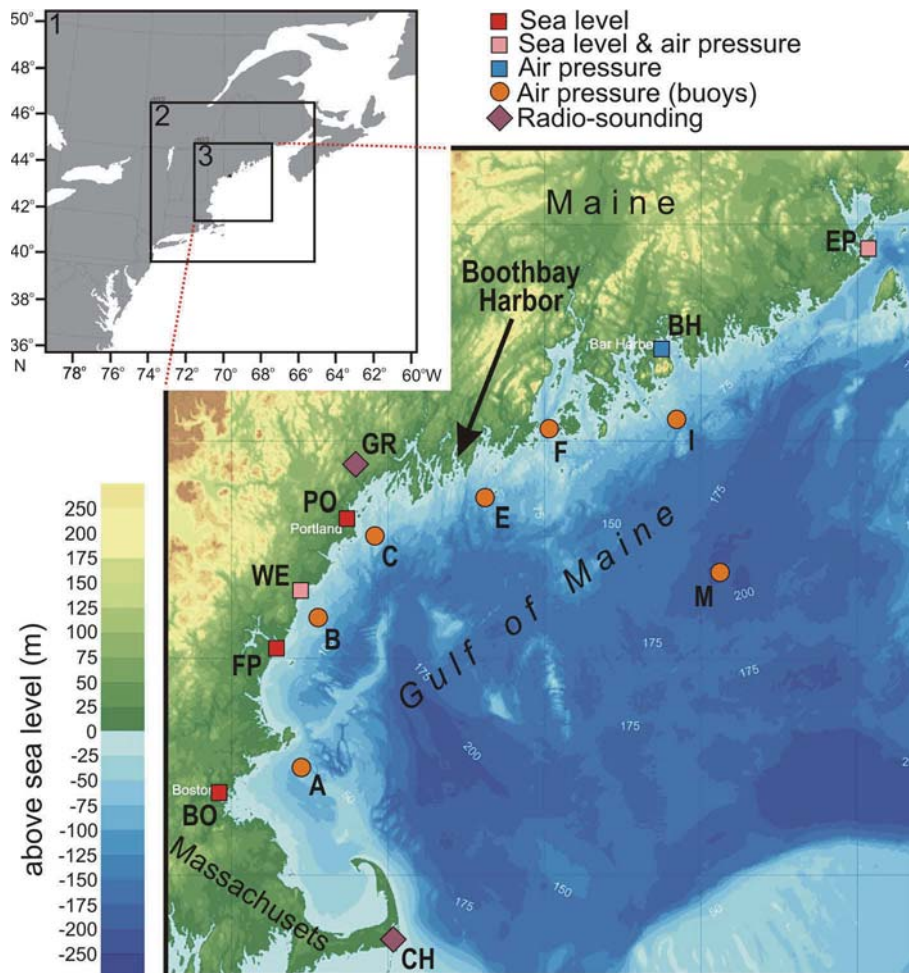
Fig. 1 Investigated area with positions of tide gauges (*squares*, *BO* Boston, *FP* Fort Point, *WE* Wells, *PO* Portland, *BH* Bar Harbor, *EP* East Port), buoys (*circles*, *A*, *B*, *C*, *E*, *F*, *I*, *M*) and sounding stations (*diamonds*, *CH* Chatman, *GR* Gray). The position of Boothbay Harbor is indicated by an *arrow*. The domains used for the WRF modelling are labelled by *1*, *2* and *3*

mid-tropospheric instability is normally associated with a convective system, stretching over several kilometres and normally observable as convective clouds by satellites (Belušić and Strelec-Mahović 2009; Vilibić et al. 2010; Renault et al. 2011). Wave-CISK presents the coupling between a gravity wave and convection, where the associated convergence forces the moist convection, while convective heating provides the energy for the wave (Lindzen 1974; Belušić et al. 2007). Both mechanisms are effective in maintaining the propagating disturbance over long distances during meteotsunamis [e.g. wave-CISK during the 2003 middle Adriatic meteotsunamis (Belušić et al. 2007) and wave duct during the 2007 Ist meteotsunami (Šepić et al. 2009)]; however, a coexistence of both mechanisms was also found during meteotsunami events (Tanaka 2010).

A reproduction of atmospheric disturbances by mesoscale atmospheric models is still under extensive research, as a slight change in model resolution, parameterization and initial conditions may strongly change the shape of the resulting ground fields (Belušić et al. 2007; Šepić et al. 2009). Renault et al. (2011) were the first to reliably reproduce a strong meteotsunami event by both atmospheric and ocean models, although the observed strength was underestimated by a factor of 2. The physics in the atmosphere were qualitatively described in a number of studies (Belušić et al. 2007; Šepić et al. 2009; Tanaka 2010), including the reproduction of both wave-CISK and wave-duct mechanisms by numerical models. The role of mountain chains has been described as well, as these are the places where initial wave perturbation has often been generated (Belušić et al. 2007; Šepić et al. 2009; Tanaka 2010; Renault et al. 2011). The atmospheric disturbances may be generated by other mechanisms as well, e.g., by convective systems and associated squall lines which may be preserved over long distances (Churchill et al. 1995), by hurricanes (Mercer et al. 2002) and in strong wind shear regions.

This paper uses all in situ and remote sensing measurements available for the Gulf of Maine event of 28 October 2008 for the quantification of witnessed high-frequency long ocean waves and their relationship to the generator in the atmosphere. Particular attention has been given to the analysis of specific synoptic conditions and small-scale features observed in the atmosphere as well as to their assessment versus existing knowledge on meteotsunami sources. The weather research and forecasting (WRF) mesoscale model was used to document the atmospheric physics lying behind the observations and to simulate specific processes observed during the event, such as rapid short-wave pressure oscillations and internal gravity waves (IGWs). Section 2 presents an overview of the observations, methods and WRF model setting; Sect. 3 establishes the relationship between high-frequency energy observed in the atmosphere and ocean and documents the relevant atmospheric processes at synoptic and local scales. Section 4 encompasses the WRF model results, including model verification and process-oriented analysis; Sect. 5 discusses the results, including an assessment of the usefulness of present observing systems and numerical models for proper reproduction of a meteotsunami source, and Sect. 6 provides the main conclusions.

2 Materials and methods

2.1 Ground ocean and meteo data

Sea-level and meteorological data were available from several observing systems located in the Gulf of Maine. Raw sea-level time series with a 1-min time resolution and a 1-mm precision measured at Boston (BO), Fort Point (FP), Wells (WE), Portland (PO) and East Port (EP) were extracted from the NOAA CO-OPS website at http://opendap.co-ops.nos.noaa.gov. Unfortunately, no tide gauges were operational in the most-affected harbours to allow a proper quantification of the reported phenomenon. The data were visually checked for spikes and other artificial errors, which were removed before the analysis. Quality-checked data were de-tided using the t-tide software package (Pawlowicz et al. 2002) and high-pass filtered by the Kaiser-Bessel digital filter.

Air-pressure data measured at WE and Bar Harbor (BH) stations with a 6-min resolution and air-pressure data measured at buoys A, B, C, E, F, I and M with a 10-min resolution were obtained from the NOAA CO-OPS and NERACOOS (http://neracoos.org) websites

and were used for quantification of the high-resolution air-pressure changes related to the travelling atmospheric disturbances. Wind data were also obtained from these stations. Vertical sounding data measured twice per day were obtained from stations Chatman (CH), Gray (GR) and Yarmouth (YA). All of the stations are illustrated in Fig. 1.

2.2 Remote sensing data

Brightness temperature data obtained from Geostationary Operational Environmental Satellite (GOES)–12 infrared window channel (10.7 μm) (NOAA CLASS system; http://www.class.ngdc.noaa.gov/saa/products/search?datatype_family=GVAR_IMG) were used in the analysis of weather conditions preceding the event. Mosaic composite radar reflectivity data originated from NEXRAD WSR-88D Doppler radars.

2.3 Speed and direction estimates of the atmospheric disturbance

The speed and direction of a propagating atmospheric disturbance from high-resolution air-pressure data have been derived following the methodology developed by Monserrat and Thorpe (1992) and applied in a number of papers (e.g., Šepić et al. 2009). The method estimates the cross-correlation function over different frequency bands from the air-pressure time series measured at any three meteorological stations deployed as a triangle. Four triangles comprising buoys close to Boothbay Harbor have been used: B-C-E, C-E-F, E-F-I and F-I-M.

Another method has been applied to the wind data measured at buoys: a version of the isochronal method (Šepić et al. 2009; Thomson et al. 2009), which assumes that the front of a disturbance is a plain wave, propagating over the area with a constant speed and direction. The method requires exact timing of the front arrival at each buoy. This was extracted from 10-min wind records (detection of the rapid change was found to be easier from the wind than from the air-pressure data).

Finally, the disturbance speed and direction were also estimated using satellite-derived Atmospheric Motion Vectors (AMVs). AMVs, also called Cloud Motion Vectors or Satellite Winds, are calculated for different atmospheric levels from subsequent satellite images in IRW and water vapour channels by comparing similar-looking, equally sized areas in the images up to a certain distance from the grid point using a standard cross-correlation technique applied to rectangular targets (Kidder and Vonder Haar 1995; Belušić and Strelec-Mahović 2009).

2.4 Atmospheric model setup

The mesoscale model used in this study is the mass-core advanced research version of the weather research and forecasting model (WRF) (Skamarock and Klemp 2008). WRF is a non-hydrostatic primitive equation model that has the terrain-following pressure as the vertical coordinate (Laprise 1992). For temporal discretization, time splitting is used to maintain the numerical stability; the low-frequency modes are integrated using the third-order accuracy integration scheme. Numerical discretization is performed on Arakawa C-grid with a fifth-order horizontal advection scheme.

The model was configured with three domains with the following horizontal grid spacings: 9 km (parent domain; referred to as 'd01'), 3 km ('d02') and 1 km ('d03') and with 41 vertical levels (cf. Fig. 1). The following physical parameterizations were chosen:

(1) the Mellor-Yamada-Janjic scheme to parameterize the turbulence in the planetary boundary layer (Mellor and Yamada 1974, 1982; Janjić 2001); (2) the Kain and Fritsch (1993; Kain 2004) scheme (dmn1 only) to represent convective processes; (3) the Eta surface layer scheme following Monin-Obhukov similarity theory (Janjić 1996); (4) the Dudhia (1989) scheme for shortwave radiation and the Rapid Radiative Transfer Model for long-wave radiation (Mlawer et al. 1997); and (5) the Morrison 2-moment microphysics scheme. The Noah land-surface model (Chen and Dudhia 2001; Ek et al. 2003) was used to simulate the vertical transport of soil moisture and heat.

The static lower boundary conditions were interpolated from the U.S. Geological Survey data sets from an arc resolution of $5'$ for d01 and $30''$ for d02 and d03. Initial and boundary conditions were provided by the operational analysis (T799 spectral truncation, roughly ~ 25 km horizontal grid resolution) of the European Centre for Medium-Range Weather Forecasts. The model simulations were initiated at 1200 UTC 28 October 2008 for a 12-h forecast range and the output data were archived every 3 min.

3 Observational evidence of a meteotsunami source

3.1 Sea-level and air-pressure high-frequency coherence

Although signal at the coastal tide gauges was entirely dominated by tides, high-frequency anomalous fluctuations became evident when tides were subtracted from raw data (Fig. 2). The largest oscillations were observed at station PO, which is closest to Boothbay Harbor (approximately 50 km), and were approximately 20 cm in range. Similar high-frequency oscillations were also recorded at stations FP, BO and WE in the afternoon hours of 28 October around 18–19 UTC. Oscillations recorded at PO were an order of magnitude lower than those eyewitnessed in Boothbay Harbor (up to 4 m), pointing to the high spatial variability of a meteotsunami, presumably caused by a complex topography and source variability. Similar high spatial variability of sea-level oscillations is often observed during meteotsunami events (Monserrat et al. 1998; Orlić et al. 2010).
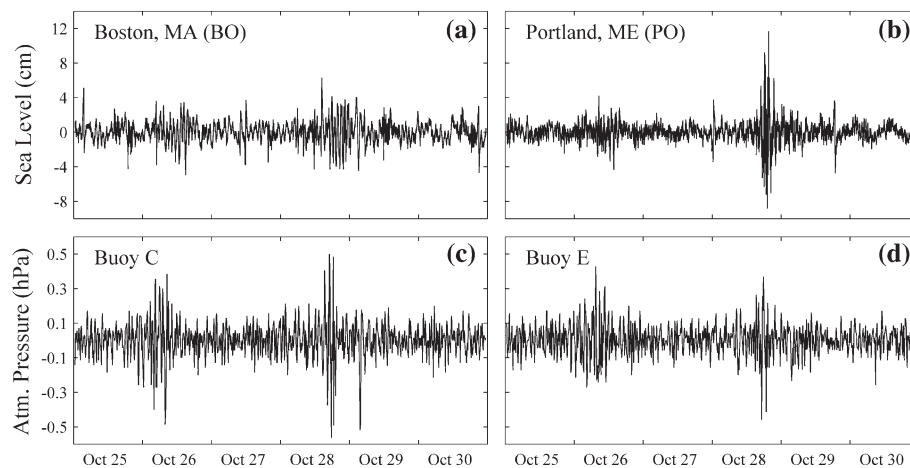

Fig. 2 High-frequency sea-level series measured at Portland (*ME*) and Boston (*MA*), and air-pressure series measured at buoys *C* and *E*. The series are filtered by 1-h moving average

No tsunamigenic earthquakes occurred and therefore may not be blamed for the observed oscillations (see USGS earthquake database at http://earthquake.usgs.gov), thus directing our search for the source mechanism to the atmosphere. Strong high-frequency air-pressure oscillations have been recorded simultaneously with high-frequency sea-level oscillations (Fig. 2). It may be observed that an intensification of high-frequency oscillations in the atmosphere coincided with observed high-frequency sea-level changes around 18–19 UTC on 28 October. On the other hand, high-frequency atmospheric oscillations recorded during the morning of 26 October did not coincide with strong sea-level oscillations. Rate of change of air pressure (temporal change over 6 min, not shown) reached a maximum on 28 October at 18–19 UTC (up to 0.1 hPa/min). The recorded rate of change is several times lower than those typically documented during destructive Mediterranean meteotsunamis (up to 0.4 hPa/min, e.g. Renault et al. 2011; Šepić and Vilibić 2011).This is likely due to the difference in air-pressure sampling resolution which was 6 times coarser for the Boothbay event (a 6-min resolution) than is usually for the Mediterranean events (a 1-min resolution) and is thus not adequate for capturing sharp pressure changes. The same problem is even more emphasized when looking at air-pressure series measured at buoys with a 10-min resolution.

The correlation between observed sea-level and air-pressure oscillations was been further investigated by means of wavelets (Fig. 3). Energy peaks visible in wavelet plots clearly show that seiche oscillations were amplified whenever an increase in atmospheric pressure energy occurred. The increase in atmospheric energy occurred on 26, 28 and 29 October and was visible over the entire frequency band; however, distinct energy maxima were found around 25 and 85 min. The 25-min period was particularly energetic during 28 October and was present at both air-pressure and sea-level spectra. The 85-min energy maximum was present during both 26 and 28 October, although the sea-level response to the second atmospheric event was much stronger than to the first one. The results from wavelets, particularly matching of the energy maxima in air-pressure and sea-level series, suggest a cause–effect relationship between high-frequency energy in the atmospheric pressure and seiche activity in the harbours. It is worth noting that energy contents in air pressure at buoy E, the one closest to Boothbay Harbor, were not particularly large in comparison with other locations. The strong response at Boothbay, therefore, cannot be simply explained by a stronger direct atmospheric forcing. Some additional aspects should play a significant role in the particular resonant amplification at this site.

## 3.2 Synoptic background and vertical structure of the atmosphere

Synoptic charts, derived from MERRA reanalysis data, document an intense quasi-stationary low-pressure system, with a centre located just southwest from the Gulf of Maine (Fig. 4a). The system underwent a rapid intensification and explosive cyclogenesis, which caused a drop in central air pressure of approximately 20 hPa from 00 to 18 UTC on 28 October 2008. The intensification was apparent throughout the entire troposphere, resulting in an intensification of southerly winds at 500 hPa height and strengthening of the jet in the upper troposphere. The winds were much weaker near the ground (Fig. 4b), where strong horizontal wind shear was found on both sides of the zone in which significant sea-level and air-pressure oscillations occurred. These zones of high shear might reflect horizontally propagating mesoscale features, keeping atmospheric energy trapped and enabling the disturbance to travel over large distances (Cheng and Alpers 2010).
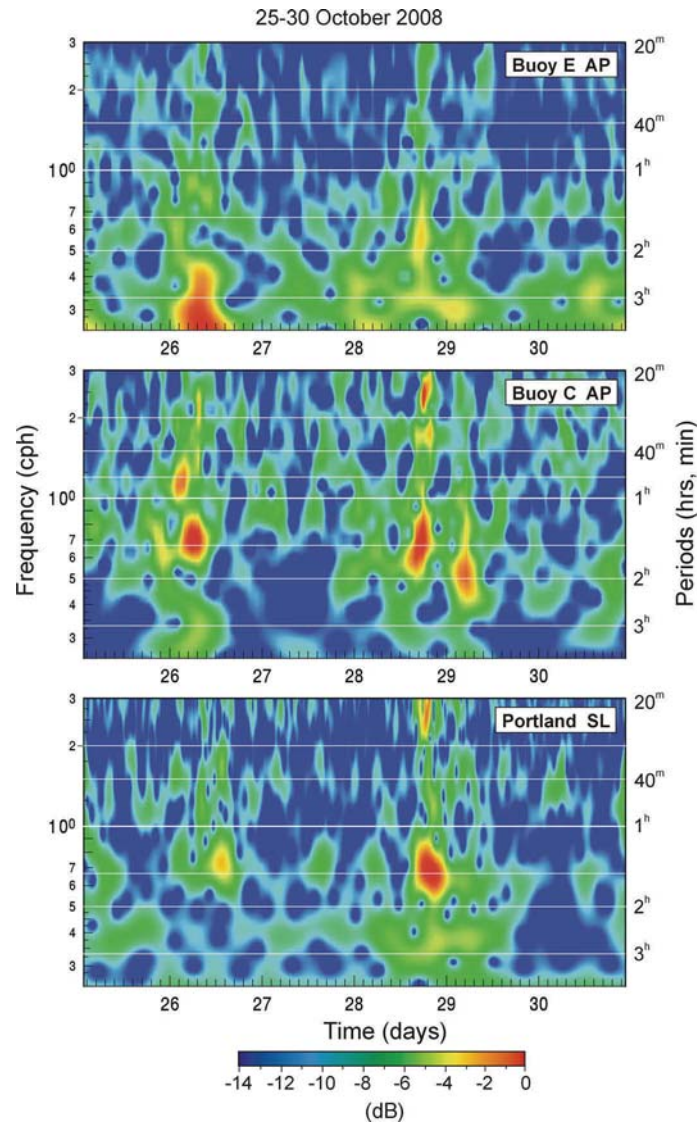
Fig. 3 Wavelets of air pressure at buoys *E* and *C* and sea level at Portland (*ME*)

In addition to horizontal energy trapping, an unavoidable characteristic of a meteotsunami is vertical energy trapping and ducting of the disturbance in lower troposphere (Monserrat and Thorpe 1992, 1996; Tanaka 2010). Vertical sounding profiles at CH and GR on 28 October 12 UTC, available at http://weather.uwyo.edu/upperair/sounding.html, revealed several temperature inversions in the first 3 km, a stable and dry air between 2 and 5 km, and an unstable layer in the mid-troposphere (between 5 and 7 km at GR and between 4 and 5 km at CH) preceding the event. The latter may serve as a reflectance layer, preventing a leakage and ducting lower troposphere disturbances over long distances.

(a)

GrADS: COLA/IGES

2012-01-07-16:37

(b)

GrADS: COLA/IGES
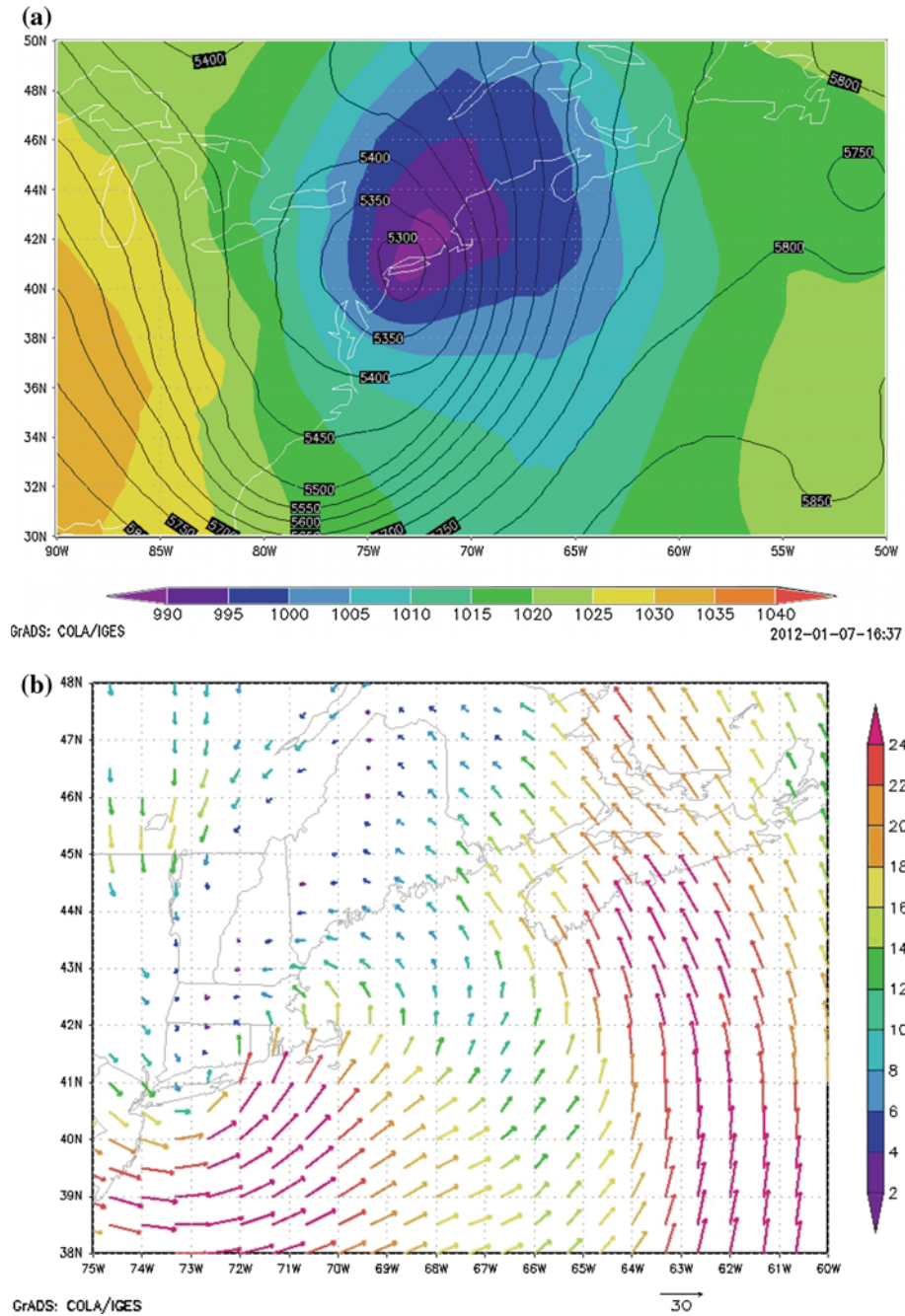
Fig. 4 MERRA reanalysis of the **a** mean sea-level pressure (*colour*) and 500 hPa height (*isolines*) data, and **b** winds at 950 hPa, for 28 October 2008, 18:00 UTC

3.3 Remote sensing analysis

Colour-enhanced infrared 10.7 μm satellite images for 28 October 2008 18–19 UTC revealed two frontal systems (Fig. 5): a cold front to the east which passed over the Boothbay region 2 days prior (on 26 October) and a cold front just passing over the region of interest. The difference between the two systems is twofold: (1) the front on the east had much colder (higher-reaching) clouds within the frontal cloud band, whereas the second front contained clouds with warmer tops, and (2) the speed of movement of the two fronts was different (the western front was catching up with the eastern one, therefore moving faster). Additionally, the system velocity of the first front had a more westerly component, with clouds moving northeastwards, while the sequence of satellite data demonstrates that the clouds of the second cold front were moving from southeast to northwest while passing over Boothbay. This movement of fronts is in agreement with the upper-level wind field (Fig. 4a). The passage of both frontal zones over the Boothbay area coincided with the timing of energy maxima in sea-level and air-pressure time series (cf. Fig 3).

A closer look at satellite images reveals a train of convective elements progressing towards Boothbay on 28 October within the frontal cloud band (Fig. 6). Convective elements in the frontal cloud band are not easily recognizable due to their rather high cloud-top temperature (the coldest tops have a temperature of about 230 °K). However, from the sequence of satellite images in Fig. 6, it can be seen that at least 3 convective cells passed over the area of Boothbay from 17:45 to 18:45 UTC, one of them (X in Fig. 6c) reaching the harbour around the time of a meteotsunami strike.
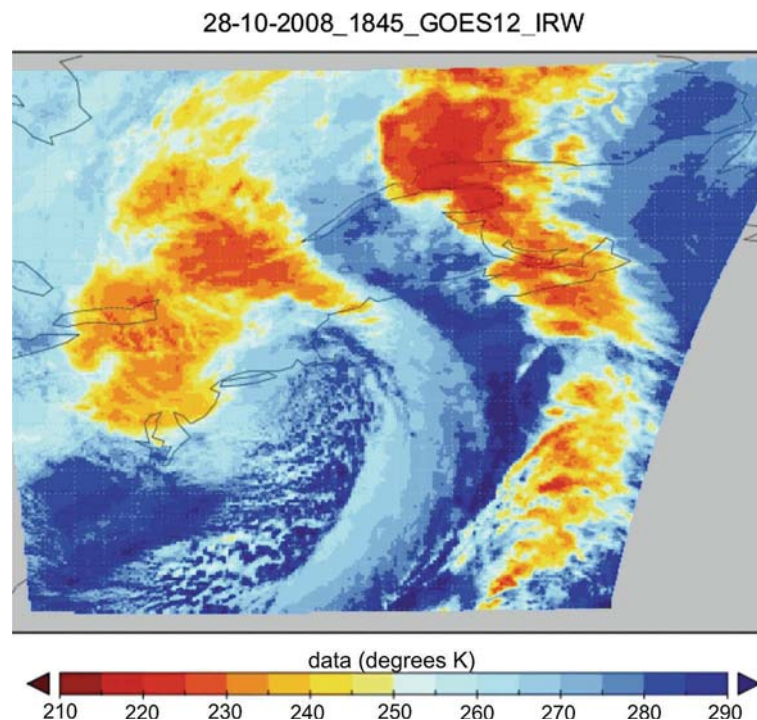
Fig. 5 Colour-enhanced GOES 12 IRW (channel 4) images for 28 October 2008 at 18:45 UTC
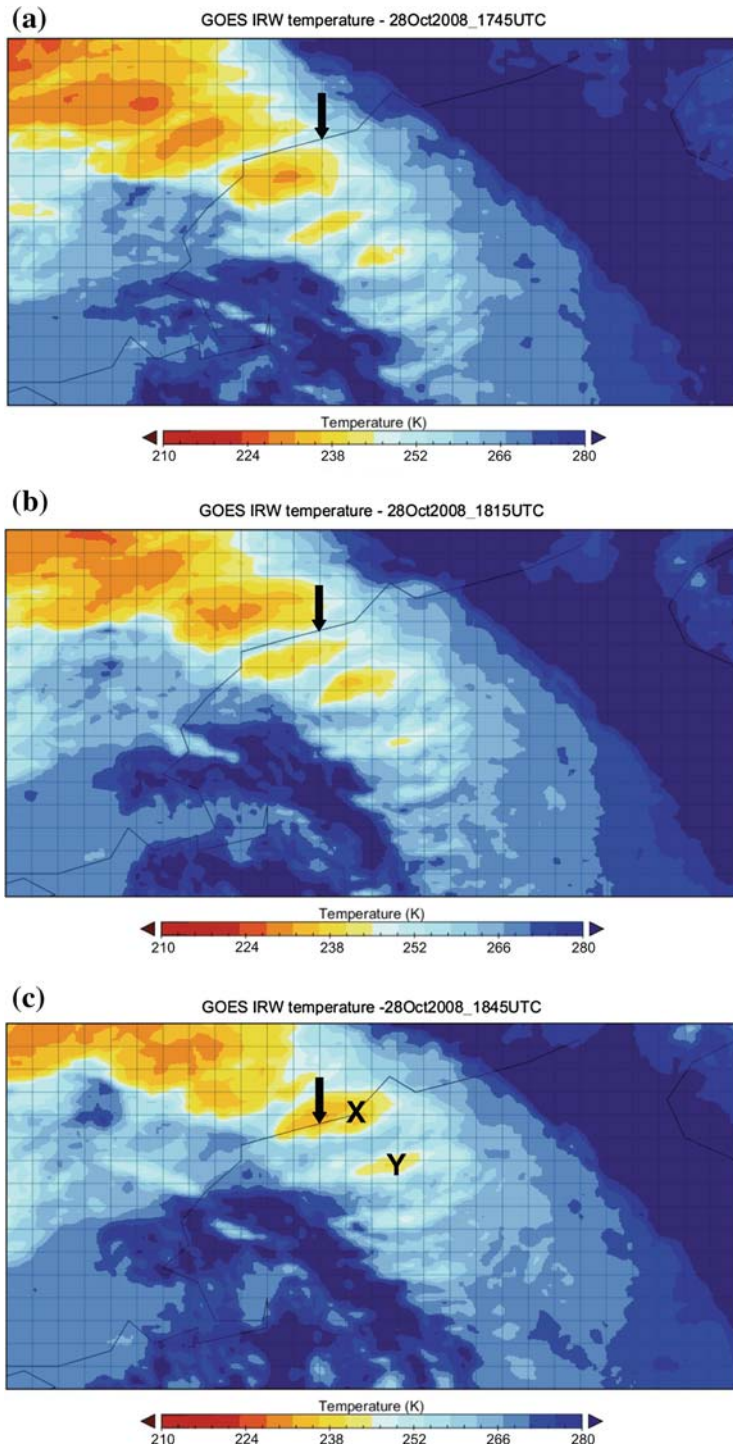
◀ **Fig. 6** Colour-enhanced GOES 12 IRW (channel 4) images for 28 October 2008 at **a** 17:45, **b** 18:15, and **c** 18:45 UTC, zoomed over the area of interest. Two convective structures are marked by *X* and *Y*, while Boothbay Harbor is marked by *arrow*

Radar images (Fig. 7) show frontal precipitation passing over Boothbay from 17:00 to 19:00 UTC (at 19:00 UTC, the front had already passed over the area of interest). From the appearance of the rain bands, it appears that there were convective clouds embedded in the frontal cloud band with a maximum reflectivity 30–50 dBZ. However, a detailed analysis of radar imagery with a 6-min interval shows that in the vicinity of Boothbay Harbor from 18:30 UTC to 19:00 UTC, reflectivity values were below 30 dBZ, demonstrating that deep convection did not occur over the Boothbay area around the time of the meteotsunami. Nevertheless, it may be noticed that individual convective cells offshore occasionally reached nearly 40 dBZ but weakened when approached the vicinity of the Boothbay area (reflectivity values below 30 dBZ). No cloud-to-ground lightning was found in the lightning data (map not shown) at the time of the event, which goes along with the observation that no deep convection took place in the vicinity of Boothbay Harbor.

Near the southeast end of the precipitation band, moist IGWs of ~ 10–15 km horizontal wavelengths approached the Boothbay area. These IGWs seen in the radar imagery were too far away from Boothbay Harbor when meteotsunami occurred to cause the event. Their existence, however, indicated that other areas associated with the back end of the precipitation zone that passed over the Boothbay area might had been prone to IGWs as well, whether or not those IGWs contained enough water droplets to be seen on the radar imagery.

The entire system moved approximately from south to north, but internal convective structures (revealed by peaks in composite radar reflectivity) had a northwestward direction (as indicated by letters P, Q and R in Fig. 7) and moved faster than the system itself. It appears that areas denoted Q and R on the radar images correspond to areas X and Y on the satellite images, respectively (cf. Fig. 6c). One reflectivity maximum (P in Fig. 7a) within the frontal cloud band reached the harbour at approximately 18:00 UTC, and another one (X in Fig. 6c and Q in Fig. 7b) reached the coast approximately 45 min later. The third convective structure denoted R in Fig. 7b (Y in Fig. 6c) passed slightly east of Boothbay Harbor shortly after 19:00 UTC. It should be noted that radar imagery generally shows much more structure than satellite imagery. This applies to areas P, Q and R, but also to other parts of the precipitation band, such as a NW–SE elongated squall line at the leading (front) edge of the precipitation band which reached reflectivity values over 45 dBZ but was not visible in the satellite data. Likewise, the moist IGWs present at the radar imagery were not visible at the satellite imagery. This highlights the inappropriateness of the analyzed satellite data for the examination of moist IGWs which have horizontal wavelengths less than ~ 15 km. The reasons for these differences are discussed in Sect. 5.

Therefore, it appears that the Boothbay meteotsunami occurred when the rear non-uniform edge of the precipitation system, with embedded convective clouds reaching 30 dBZ, just moved over the area, immediately followed by an environment potentially susceptible to IGW propagation.

3.4 Disturbance speed and direction estimates

The estimates of speed and direction of atmospheric pressure disturbance, obtained with the triangular method, are shown in Table 1. Depending on a cut-off frequency, a different number of triangles satisfy the quality requirements necessary for the assessment of speed
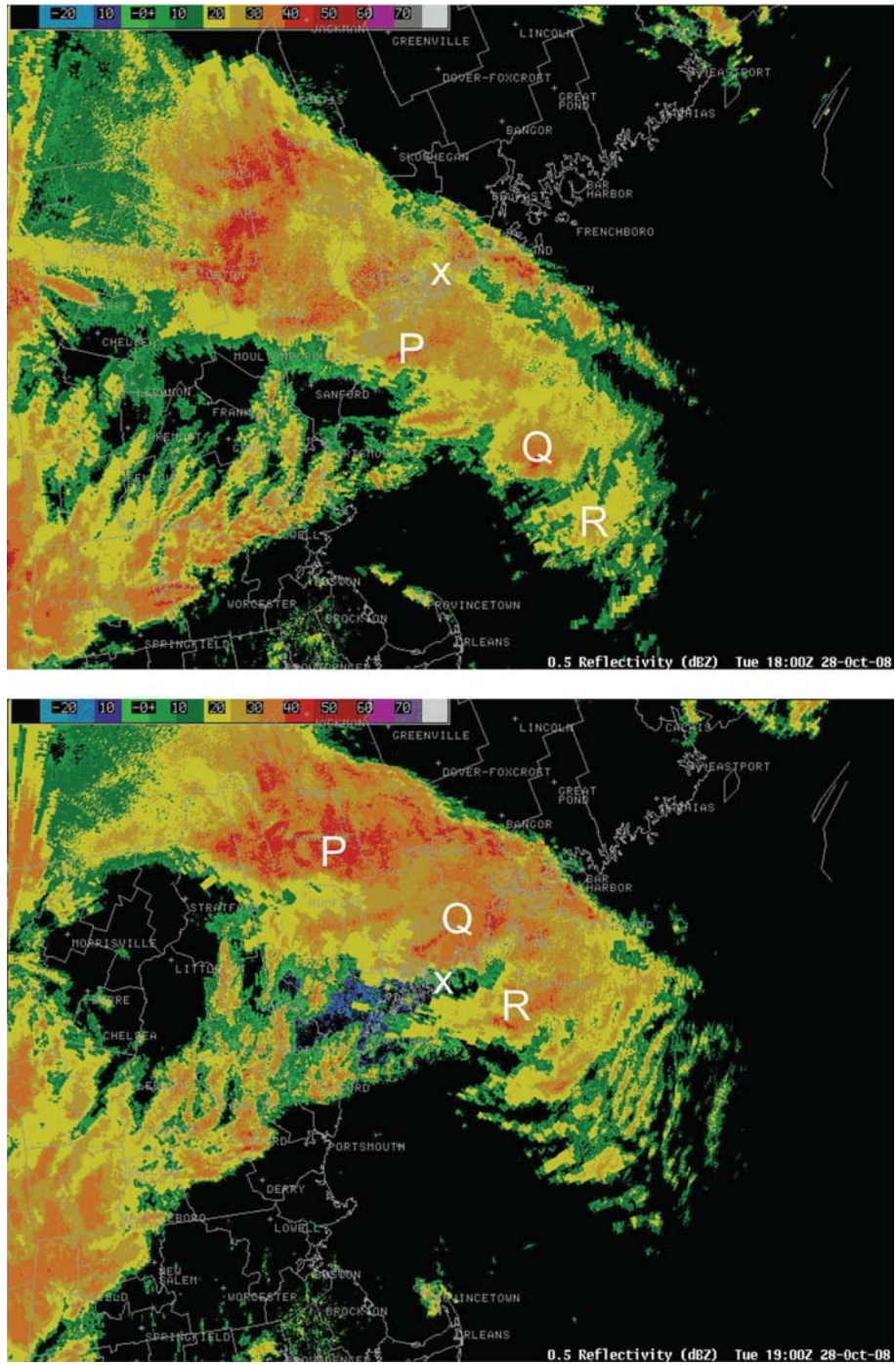
Fig. 7 Composite radar reflectivity (dBZ) on 28 October 2008 at 18 UTC (*top*) and 19 UTC (*bottom*). Letters P, Q and R denote the movement of the individual convective structures within the precipitation band (inferred from animations, 6-min data frequency). The position of Boothbay Harbor is marked by cross

Table 1 Phase speed (*c*) and direction (α) of the atmospheric disturbance obtained from triangles of air-pressure data

	Tri. E-F-I	Tri. C-E-F	Tri. F-I-M	Tri. B-C-E
5-h-filtered				
c (ms^{-1})	23.7	37.7	–	–
α (°)	345.0	22.5	–	–
12-h-filtered				
c (ms^{-1})	29.5	26.6	23.8	24.0
α (°)	355.4	14.2	175.4	55.8

For wave direction, an oceanographic criterion has been used, where zero degrees indicates waves travelling towards the north

and direction. When the cut-off frequency is set to 5 h, only two triangles satisfy quality criterion, but results of estimates are not consistent (speed of 24–38 ms^{-1}; azimuth direction between 345° and 23°). When the cut-off frequency is increased to 12 h, the results for speed became coherent (24–29 ms^{-1}), but the direction estimates are still not reliable (350°–175°). The available data suggest that perturbations on the order of several hours travelled above the region with phase speeds of approximately 24–29 ms^{-1} and with the direction azimuth 340°–50° (towards NNW to NE). When the data were filtered to retain only those oscillations of the order of minutes, the correlations found between stations were not adequate to compute the atmospheric wave characteristics.

These inconsistencies are largely a result of the distance between stations being too large, the stations being in alignment and the time sampling being too coarse to properly analyze high-frequency perturbations.

By assuming a plain wave shape of the disturbance and introducing wind instead of air-pressure data, the speed of the travelling wind disturbance was estimated to be 17.3 ms^{-1} at a direction towards the north. However, 10-min wind data (as for air pressure) were not of sufficient resolution and could not properly capture disturbances embedded in the frontal zone possibly moving with different speeds and directions; this method only captures the movement of the front as a whole. Additionally, wind is usually found to be very weak or to last for only a few minutes during meteotsunamis (Vilibić et al. 2004; Jansà et al. 2007).

The most coherent estimate of disturbance speed and direction was attained from the cloud-top motion velocity. The speed was estimated to be 30–32 ms^{-1}, which is somewhat larger than the phase speed of the atmospheric waves estimated from the pressure gauge data. The propagation direction near Boothbay Harbor was towards 320° (NW), which is in agreement with previous analyses. Similar findings, i.e., cloud-top velocity higher than the velocity of a ground disturbance, were documented for other meteotsunamis. (e.g. the 2007 Black Sea meteotsunami, Vilibić et al. 2010). This is a result of an increase in wind speed with height which is in turn a prerequisite for an efficient ducting of waves in the lower troposphere (Monserrat and Thorpe 1996).

4 Atmospheric modelling

The observational evidence suggests that the source of observed sea waves was atmospheric internal gravity waves. In this section, we assess the presence and maintenance of IGWs with high-resolution numerical simulations using the mesoscale WRF model.

4.1 Model verification

Verification of the WRF model simulation was performed using buoy, radio-sounding, remote sensing and reanalysis data. The sub-synoptic decrease in air pressure associated with the approaching cyclone and the precipitation band were satisfactorily simulated with errors mainly below 1 hPa; only at the Wells station did errors reach 2 hPa (Fig. 8a). Furthermore, a comparison of the high-resolution model output (archived each 3 min) with the observations (available each 10 min) at the two stations closest to the location of the meteotsunami (insert of Fig. 8a) suggests that the two regimes of measured air-pressure changes in the Boothbay area were also simulated. First, until 17:00 UTC 28 October 2008, both the observed and modelled pressure series were relatively uniform with no abrupt oscillations. From 17:00 UTC–19:00 UTC 28 October 2008, the measured increase in air-pressure variability observed at the buoy E was quantitatively simulated with a time-lag of less than half an hour. It appears that the frequency of measured data is sub-optimal and sufficient neither for an in-depth analysis of the high-frequency air-pressure oscillations as those ones associated with the Boothbay meteotsunami nor for a quantitative verification of the air-pressure variability of the WRF model results.

A comparison of the WRF results with the radio-sounding data at station GR (verification on stations CH and YA not shown) showed that the simulated vertical profiles of temperature, dew-point temperature and wind speed and direction generally agreed well with the observations (Fig. 8b). Nevertheless, the simulated mid- to upper-tropospheric dew-point temperature and mid-tropospheric wind speeds were overestimated; however, these errors are of moderate amplitudes. As inferred by the comparison of the WRF results and the MERRA and ERA-Interim reanalysis data, the model performed well in simulating the cyclone southwest of the Boothbay area (not shown). This was expected considering the short simulation horizon (the meteotsunami occurred approximately 9 h after the model initiation time).

The simulation of the precipitation band, which moved over the Boothbay area in minutes preceding the meteotsunami event, was verified by using the observed and simulated radar reflectivity images (Fig. 9, cf. Fig. 7). Modelled radar reflectivity was calculated with constant intercept parameters for the size distributions of rain, snow and graupel (Reisner et al. 1998).
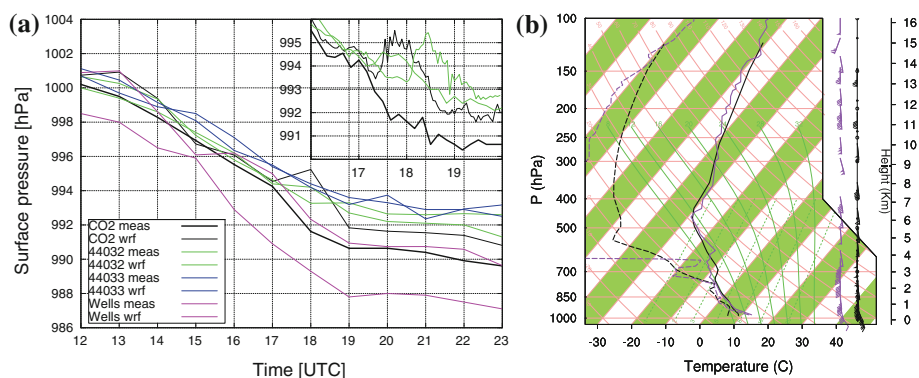
Fig. 8 Measured and modelled time series of **a** air pressure at buoys C (C02), E (44032), F (44033) and Wells from 12:00 UTC 28 October 2008 to 23:00 UTC 28 October 2008 with hourly frequency. The *inset* shows measured and modelled time series from 16:00 UTC 28 October 2008–20:00 UTC 28 October 2008 with 10 and 3-min frequencies, respectively, at the two closest buoys to Boothbay Harbor. **b** Measured (*purple*) and modelled (*black*) vertical soundings at 00:00 UTC 29 October 2008 at Gray station
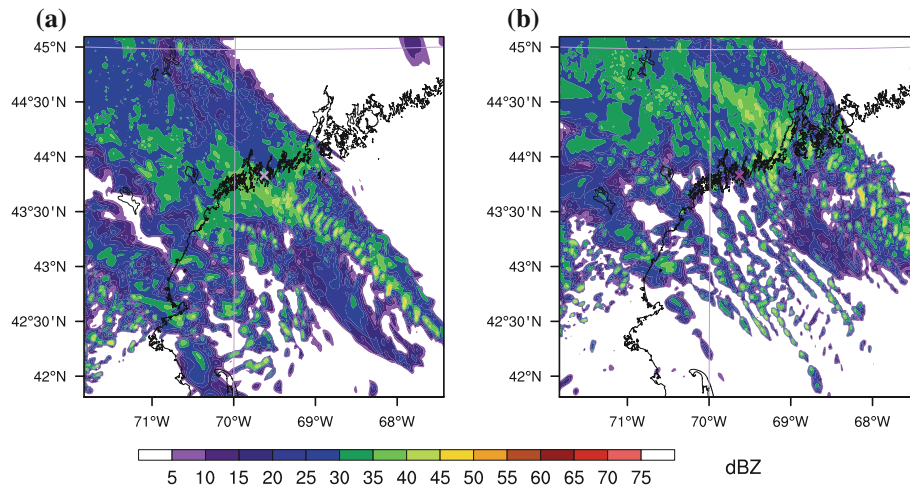
Fig. 9 Simulated maximum radar reflectivity on 28 October 2008 at **a** 18:00 UTC and **b** 19:00 UTC. The position of Boothbay Harbor is marked by a *gray* cross

Generally, the simulated radar reflectivity associated with the passage of the precipitation band resembled the measured radar reflectivity, with simulated reflectivity values reaching over 40 dBZ. At both 18:00 UTC and 19:00 UTC 28 October 2008, the shape of the precipitation band, its intensity and the position of its leading edge were relatively accurately simulated. However, a more detailed analysis revealed some deficiencies in the simulation: (1) the weak convective activity observed south of the precipitation band and east of Massachusetts Bay was overestimated in the model; (2) the individual convective areas denoted P, Q and R and the associated convective sub-structures of each of those areas on the radar imagery were not easily identifiable in the simulation; and (3) the wave-like pattern of the radar reflectivity near the southeastern edge of the precipitation system (see Sect. 3.3) was not accurately simulated. The (1) and (3) are not of major importance because at the time of the meteotsunami, both the weak convective activity south of the precipitation band and the moist IGWs found in the radar imagery were too far offshore from Boothbay Harbor to be related to the meteotsunami. While we recognize that the analysis of convection may be of interest for this event, we note that the gross features of the precipitation band were relatively precisely simulated, but that accurate simulation of position and intensity of individual convective cells is often challenging for mesoscale models. Furthermore, we note that there was no deep convection in the very Boothbay area, which decreases the likelihood for convectively generated intense surface pressure oscillations. To summarize, although the southern edge of the precipitation band was simulated with lower accuracy than its northern edge, the mesoscale numerical simulation is considered useful for a more detailed analysis of the atmospheric conditions prior and during the time of the meteotsunami.

4.2 Reproduction of meteotsunami source

4.2.1 The surface pressure distribution

Simulated mean sea-level pressure suggests that the moving precipitation band was associated with the high-pressure band (Fig. 10). The 50-km-wide pressure band was elongated from northwest to southeast and propagated northward, and its advection time
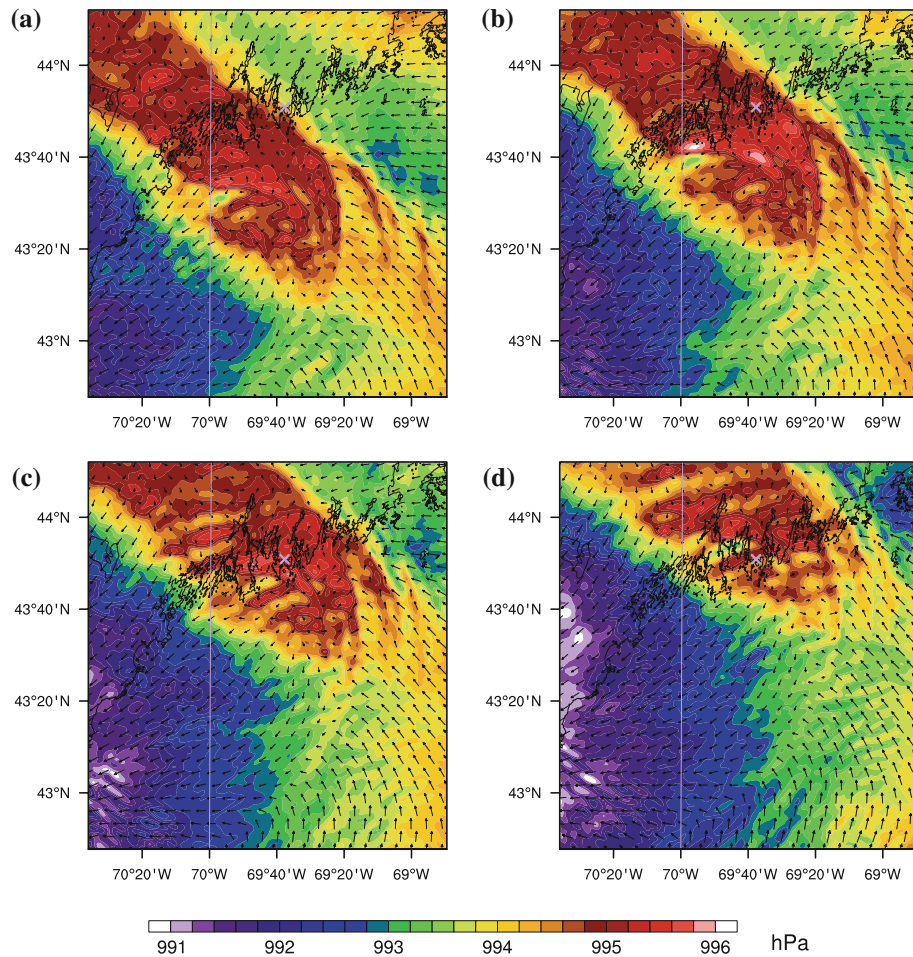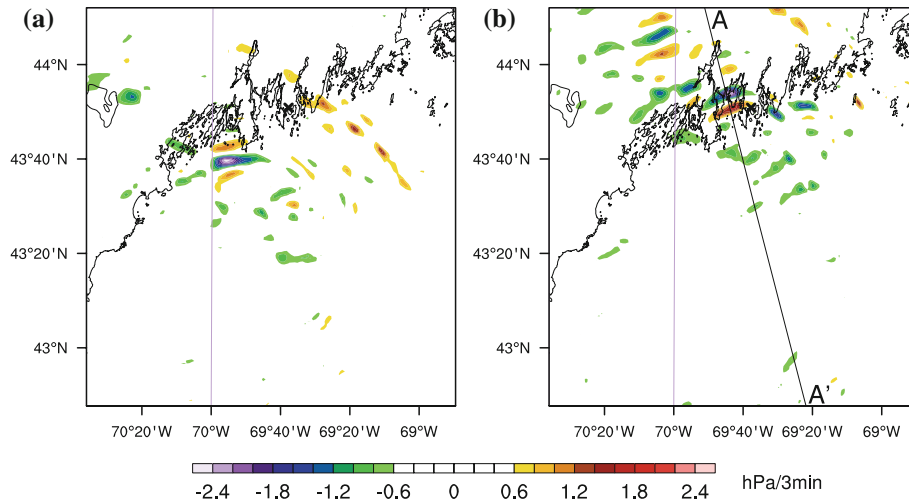
Fig. 10 Simulated mean sea-level pressure and 10 m wind vectors on 28 October 2008 at **a** 18:06 UTC, **b** 18:18 UTC, **c** 18:30 UTC and **d** 18:42 UTC. The position of Boothbay Harbor is marked by a *gray* cross

scale was close to 35 min. The front end of the disturbance reached Boothbay Harbor around 18:06 UTC according to the model simulations (Fig. 10a), causing a pressure increase of ~2 hPa. Such 'pressure jumps' are common features of meteotsunamis; however, the remote sensing analysis suggested that the meteotsunami occurred near the back edge of the precipitation band.

Near the rear edge of the high-pressure band, the pressure decrease was generally not as sharp as it was near its leading edge. Even prior to 18:00 UTC, localized high-frequency pressure oscillations were simulated near the back end of the precipitation band over the Gulf of Maine which by 18:06 UTC reached an amplitude of 2 hPa (Fig. 10a). In subsequent minutes, the pressure oscillations intensified, attained amplitudes as high as 3 hPa, and propagated towards the NNW (Fig. 10b). According to the simulation, by 18:18 the first pressure oscillations hit the shore approximately 30 km west of Boothbay Harbor. In the next minutes, the location where pressure oscillations reached the coast moved eastward towards Boothbay Harbor (Fig. 10c). Intense pressure oscillations were simulated
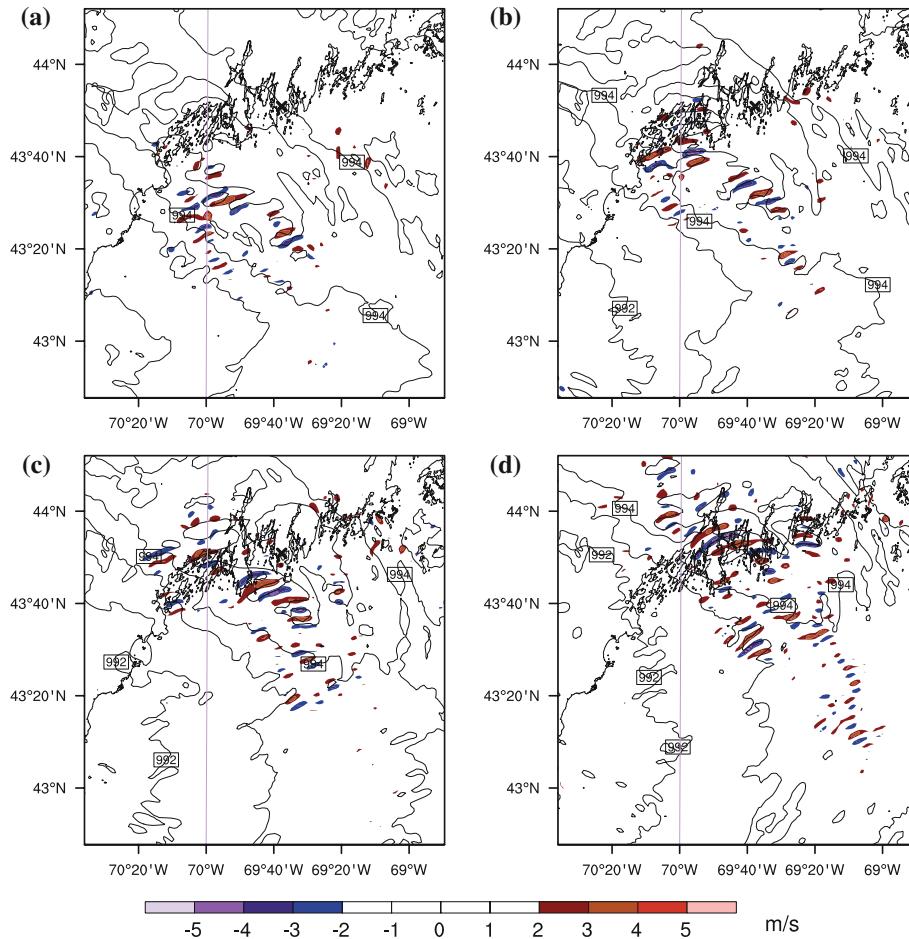
Fig. 11 Simulated mean sea-level pressure tendencies (hPa/3 min) on 28 October 2008 at **a** 18:18 UTC and **b** 18:42 UTC. The position of Boothbay Harbor is marked by a *black* cross, and the cross-section used in Figs. 13 and 14 is denoted AA′

near Boothbay Harbor around 18:42 and in subsequent minutes (Fig. 10d), which approximately corresponds to the time of the reported meteotsunami (around 19:00 UTC). At that time, the most intensive pressure oscillations had amplitudes greater than 2.5 hPa and wavelengths of 10–12 km. In the entire pressure pattern, the most intense pressure oscillations were simulated slightly to the west of Boothbay Harbor. Eventually, the oscillating pressure system crossed the Boothbay area and moved farther to the north, where it gradually dissipated.

The pressure oscillations impinging on the coast were closely tied to the southern end of the precipitation band and occurred in zone of a 15–30 km transverse width. This finding is more clearly depicted by the simulated rates of change of mean sea-level pressure which were calculated over 3-min time intervals, which is the chosen archival data frequency for the model. During the event, the rates of change of air pressure continuously reached absolute values of 2 hPa/3 min in the Boothbay area (Fig. 11a,b), with maximum tendencies over 2.5 hPa/3 min. While the simulation suggested the existence of two primary pressure oscillation packets, the observational evidence was not sufficient to evaluate this result. For this reason, we did not analyze the properties of each of these oscillations individually. Finally, the constrained horizontal width of the pressure oscillations suggests that the wave packets in the event were generated by a local process and laterally trapped. This was already suggested by analysis of satellite images and wind data. In addition, small wavelength of atmospheric pressure oscillations and constrained width suggest why the most intensive atmospheric pressure oscillations were not observed at the nearby buoys.

The presence of an oscillating pressure pattern near the back edge of the precipitation band in the simulation, approximately at the same time when the Boothbay meteotsunami occurred in the vicinity of the observed back edge of the precipitation system, suggests these surface pressure oscillations were associated with this meteotsunami. Additional discussion of this issue will be provided in Sect. 5.

Fig. 12 Simulated vertical velocity at 2.6 km AGL (*shaded*) and mean sea-level pressure (contours) on 28 October 2008 at **a** 18:06 UTC, **b** 18:18 UTC, **c** 18:30 UTC and **d** 18:42 UTC. The position of Boothbay Harbor is marked by a *black* cross

4.2.2 The presence and propagation of internal gravity waves

The observational analysis and the simulated oscillating mean sea-level pressure pattern suggest an oscillatory nature of the atmospheric field. As inferred from the simulation, at as early as 17:00 UTC on 28 October 2008, mid-tropospheric wave packets of IGWs were created near the back southeastern edge of the precipitation band (not shown). As the precipitation band moved northward, new wave packets were continuously created near its rear edge. At 18:06 UTC, the first intense wave packets of IGWs, easily detectable in vertical velocities profiles, approached the area (Fig. 12a). The wavelength of IGWs was 10–12 km, and the absolute vertical velocities (being a measure of IGW strength) at 2.6 km above ground level (AGL) were over 3 ms^{-1}. In the subsequent minutes, the IGWs intensified and propagated towards the NNW (NW), reaching the coast west of Boothbay Harbor (Fig. 12b). Subsequently, the system approached the shore, and by 18:30 UTC on
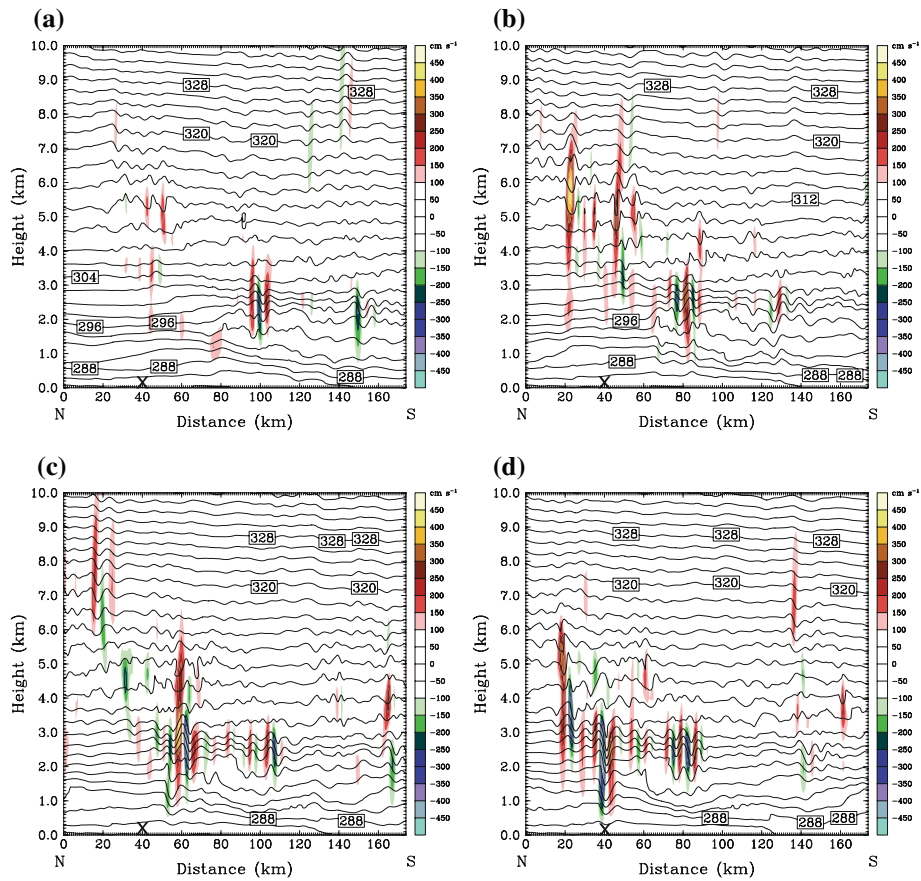
Fig. 13 Potential temperature (contours) and vertical velocity (*shaded*) over AA' section (cf. Fig. 11), on 28 October 2008 at **a** 18:00 UTC, **b** 18:30 UTC, **c** 18:42 UTC and **d** 18:54 UTC. The position of Boothbay Harbor is marked by a *black* cross

28 October 2008, a coherent wave packet of IGWs almost reached Boothbay Harbor (Fig. 12c). In the next quarter an hour, the wave packet propagated over the Boothbay area towards inland (Fig. 12d), followed by less intense wave packets of IGWs still offshore. Finally, after the group of wave packets crossed the Boothbay area, the entire system propagated northward and dissipated farther inland.

The vertical structure of the wave packet of IGWs that caused intense surface pressure oscillations to cross Boothbay Harbor is shown in Fig. 13. At 18:06 UTC on 28 October 2008, this isolated wave packet was located ~ 70 km offshore off the Boothbay area (Fig. 13a). As observed from the vertical sections, this wave packet was confined to the mid-troposphere with the largest amplitudes somewhat below 3 km AGL. The wave packet propagated towards the shore with a propagation speed of approximately 28 ms^{-1}. In the subsequent minutes, the wave packet acquired a more coherent and weakly dispersive character, and its phase speed was 2–30 ms^{-1} (Fig. 13b). The internal gravity waves in the packet clearly propagated downwards towards the ocean. At the same time, intense IGWs

were also found above 4 km AGL closer to the shore and over Boothbay Harbor. However, those IGWs were dispersive and quickly disappeared.

While the wave packet approached Boothbay Harbor and intensified, its propagation speed remained unchanged (Fig. 13c). The absolute vertical velocities reached nearly 5 ms^{-1}, and the waves occasionally steepened to the overturning and wave-breaking level. At 18:42, the most intense part of the wave packet had just propagated over Boothbay Harbor (Fig. 13d). The wave amplitudes were confined to depths below 3.5 km, with a clear indication of wave-induced near-surface potential temperature and pressure perturbations. Therefore, the coherence of IGWs in the middle troposphere and oscillating surface pressure system suggest surface pressure oscillations were closely tied to IGWs aloft.

The potential for downward (or upward) propagation of mid-tropospheric IGWs may be assessed from the following inequality of the linear gravity wave theory (e.g., Lin 2007):

$$N > \frac{2\pi U}{\lambda} \qquad (1)$$

where N is the Brunt-Väisälä frequency, U is the mean horizontal wind speed and λ is the horizontal wavelength of IGW. Estimation from simulations yields values of $N = 0.014$ s^{-1}, $U = 20$ ms^{-1} and $\lambda = 11$ km, (thus giving $2\pi U/\lambda = 0.011$ s^{-1}) which satisfies the required condition. This finding suggests that the wave packet was in an environment where it could propagate vertically (both up and down), provided that no reflection or absorption levels, such as inversions or critical levels, prevented the vertical propagation, which we will discuss further in the next sub-section. For this reason, the wave packet propagated down towards the ocean surface.

The horizontal wavelength of mid-tropospheric IGWs as well as their speed and direction of propagation corresponded exactly to the properties of the surface pressure oscillations. The surface pressure oscillations (as well as the mid-tropospheric pressure perturbations) and vertical velocities in the wave packet differed in phase for ¼ of the wavelength, which is a distinct property of internal gravity waves (Nappo 2002). The direction of the IGW propagation also corresponded well to the direction of atmospheric perturbance found by triangularization estimates from the air-pressure series and to estimates from satellite analysis. Finally, the wavelengths of simulated IGWs are similar to the wavelengths of the moist IGWs observed in the radar imagery. Therefore, it can be presumed that the surface pressure oscillations and the Boothbay meteotsunami were caused by a weakly dispersive wave packet of IGWs.

4.3 The maintenance of internal gravity waves

For a meteotsunami to occur due to coupling of IGWs with the ocean surface, IGWs need to be maintained over at least several wave periods (Monserrat and Thorpe 1996). Indeed, as mentioned in the former section, the weakly dispersive mid-tropospheric wave packets of IGWs that caused intense surface pressure oscillations near Boothbay originated well before they reached the harbour. In these circumstances, a maintenance mechanism, such as wave-duct of wave-CISK, must exist and compensate for the energy coherence loss due to dispersion.

According to the linear wave-ducting mechanism (Lindzen and Tung 1976), linear mesoscale internal gravity waves can be ducted in the lower troposphere under the following conditions: (1) a stable layer of air in which the waves can propagate is near the ground, (2) this stable layer is topped by a sheared unstable layer with Richardson number
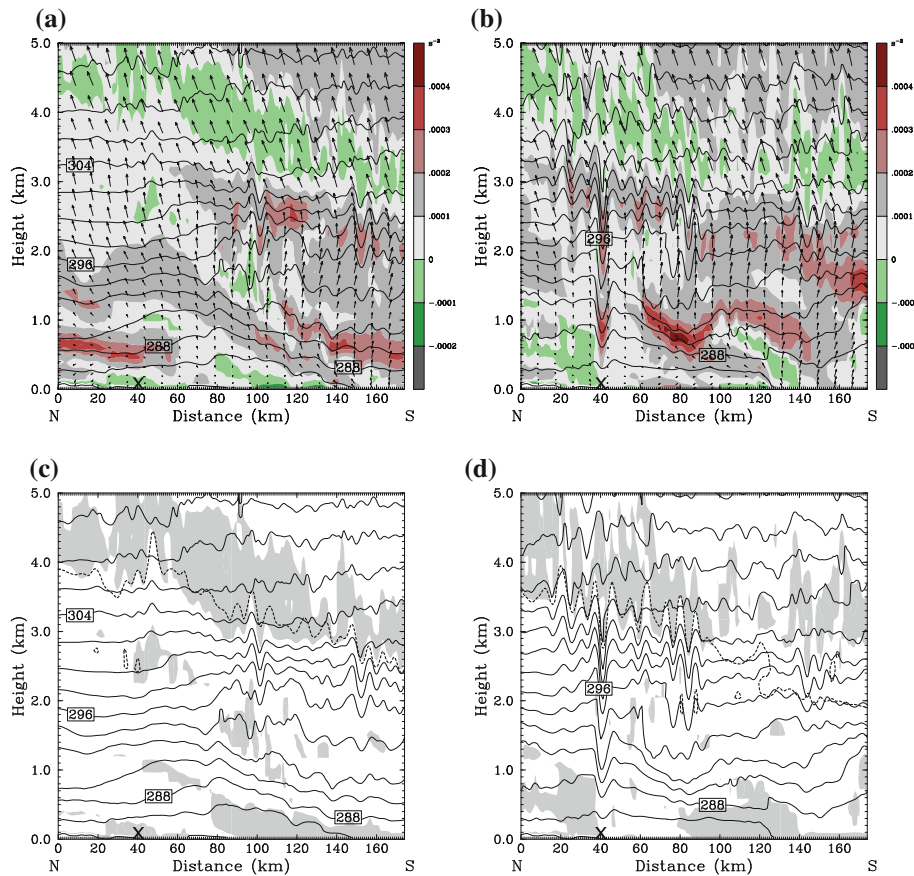
Fig. 14 Simulated potential temperature (contours), moist Brunt-Väisälä frequency (*shaded*) and *horizontal* wind vectors over AA′ section (cf. Fig. 11) on 28 October 2008 at **a** 18:06 UTC and **b** 18:42 UTC, and simulated potential temperature (contours), Richardson number (*shaded below* 0.25), the isotach of 29 ms^{-1} of the section-parallel wind speed component (*thick dashed* contour), on 28 October 2008 at **c** 18:06 UTC and **d** 18:42 UTC. The position of Boothbay Harbor is marked by a *black* cross

$Ri < 0.25$, (3) there is an embedded critical level in the unstable layer aloft and (4) the depth of the wave-duct D is

$$D = \lambda_z(1/4 + 1/2n), \qquad (2)$$

where λ_z is the vertical wavelength and $n = 0, 1, 2, \ldots$ We note that the criterion (4) is often overlooked in studies of ducted IGWs (e.g. Lin 2007), which also applies to some studies related to meteotsunamis.

The analysis of the simulated Brunt-Väisälä frequency suggests a multilayer structure of the troposphere over the Gulf of Maine (Fig. 14). The stable layer was adjacent to the ocean surface and capped by the unstable air, which was again topped by the stable air aloft in the upper troposphere. At 18:06 UTC, the height of the stable layer decreased from 4 km AGL in front of the precipitation band to 3–3.5 km AGL near the wave packet (Fig. 14a). Behind the wave packet, the depth of the stable layer decreased. At that time, several areas of unstable air were embedded within the stable layer below and around the wave packet,

but in the next minutes, these areas almost disappeared. By the time the wave packet which was initiated around 18:00 UTC reached Boothbay Harbor around 18:42 UTC, it acquired a notably pronounced and coherent structure with no vertical tilt throughout the lower and middle troposphere (Fig. 14b). Above that level, the coherence of the packet disintegrated, apparently in the unstable layer capping the layer of wave propagation below.

The winds at IGW's critical level equal their phase speed, which was approximately 28–30 ms^{-1}. In the early phase of formation of the wave packet that reached Boothbay Harbor, the critical level was entirely within the dynamically unstable layer of $Ri < 0.25$ (Fig. 14c). Therefore, this critical level acted as a reflector of the incident wave energy and trapped the internal gravity wave packet below (e.g., Lin 2007). Furthermore, the required depth of the duct D may be estimated from Eq. (2) using simulated average values of N (0.014 s^{-1}), U (21 ms^{-1}) and c_p (29 ms^{-1}) and approximating $\lambda_z = 2\pi(c_p - U)/N$, where c_p is the phase speed, U is mean wind speed and N is the Brunt-Väisälä frequency. The estimation yields $D = 3.5$ km, which roughly corresponds to the simulated depth of the stable layer. Therefore, the four necessary conditions for the wave duct were fully satisfied during the wave packet propagation towards the Boothbay area.

The critical level remained embedded in the dynamically unstable layer in the subsequent period of wave packet propagation towards the shore. By the time the most intense part of the wave packet crossed Boothbay Harbor (Fig. 14d), the unstable capping layer slightly disintegrated; however, most of the wave packet was still capped by the unstable layer and the critical level within. In the subsequent period, disintegration of the capping layer continued increasing the dispersive properties of the wave packet. Therefore, the conditions required for a wave duct were simulated starting from the initiation of the IGWs until the time when the wave packet moved farther onshore from the Boothbay area.

Therefore, the analyzed wave packet was trapped from above but propagated downward towards the ocean, causing intense near-surface pressure oscillations. Notably, not all simulated wave packets propagated downward to the ocean surface. For example, an intense wave packet that occurred at 18:42 and was located approximately 40 km offshore of Boothbay (cf. Fig. 13d) did not have a signature of surface pressure oscillations (cf. Fig. 10d). Namely, in addition to the capping from above, this wave packet was trapped from below by the strong inversion that was simulated below 1 km AGL (Fig. 14b). Therefore, an efficient propagation of the ducted mid-tropospheric IGWs towards the surface is essential for causing intense pressure oscillations near the surface.

5 Discussion

The analysis of the 2008 Boothbay meteotsunami event revealed a number of characteristics of a meteotsunami: (1) it occurs quite rarely and has a destructive intensity, as it is a multiresonant phenomenon; (2) it occurs abruptly as a tsunami, causing a panic to the population; (3) it has the maximum strength in deep harbours and bays, where settlements are normally located; (4) it is often associated with convective systems, although not with the strongest, but with the ones having a specific rate of air-pressure change; (5) the source has quite strong spatial and temporal variability that is very hard to capture at present through currently available observational meteo and ocean systems; and (6) the underlying atmospheric physics are quite challenging to reproduce mostly due to grid spacing and parameterization schemes of the present state-of-the-art mesoscale atmospheric models.

Although this study does not attempt to reproduce the observed meteotsunami waves in the ocean and is focused on the assessment and reproduction of a source in the atmosphere,

all observed data classify the phenomenon as a meteotsunami (Monserrat et al. 2006): (1) rapid changes of air pressure and wind were detected by the observation systems at the time of observed ocean waves and reproduced by the atmospheric model to occur over the sea in front of the Boothbay area; (2) ocean depths in front of the Boothbay area are favourable for efficient energy transfer from the atmosphere to the sea through the Proudman resonance (Proudman 1929); namely, the disturbance moved towards N-NNW with a speed of approximately 28–30 ms^{-1}, travelling largely over waters with depths of 80–100 m where resonant effects are strongly manifested.

The open-ocean resonance and matching of energy maximum period at 25 min (cf. Fig. 3) with eyewitnessed oscillations with period of about 20 min is probably the reason why the Boothbay Harbor and surrounding areas were hit by meteotsunami waves. An elongated shape of the Boothbay Harbor indicates strong amplification factor of incoming waves (Rabinovich 2009); furthermore, incoming direction of the atmospheric disturbance and presumably ocean wave direction match the principal axis of the bay. This could be further confirmed for the Boothbay area by conducting targeted ocean numerical modelling with variable atmospheric pressure disturbance intensity, speed and direction.

Two frontal zones hitting the area on 26 and 28 October 2008 indicate that the atmospheric events with increased air-pressure energy are common in the area; nevertheless, the event on 26 October was less energetic in the air-pressure series and much weaker in the sea-level series. In particular, the presence of the 25-min air-pressure energy maximum on 28 October and its absence on 26 October was presumably the most important difference between them, as no energy was transferred to the ocean on 26 October at eigenperiods of the Boothbay Harbor and surrounding area. Air-pressure disturbances with large energies at short periods normally occur only during intense and small-scale processes like sharp frontal zones, squall lines, IGWs and similar. As these processes are normally dissipative at small spatial scales and may be maintained over a large area only during very specific conditions (wave-duct and wave-CISK conditions, see Monserrat and Thorpe 1996; Belušić et al. 2007), a destructive multiresonant event like the one observed on 28 October occurs very rarely.

Available ground, tide gauge and buoy observations were not sufficient to properly capture both ocean waves and atmospheric parameters. The tide gauge at Portland, located 50 km SW from Boothbay Harbor, recorded only 20 cm meteotsunami wave heights, pointing to the high spatial variability of the phenomenon. A number of buoys recorded a sharp change in air pressure and wind at the time of the meteotsunami; nevertheless, the rate of change of air pressure was several times smaller than the one usually recorded during documented meteotsunamis. This holds even for the buoy E placed close to the front of Boothbay Harbor (Jansà et al. 2007; Šepić and Vilibić 2011). The series was recorded with 10-min resolution, which was found to be inadequate for properly detecting the strength of the atmospheric forcing; the sampling should be performed at least every minute (Monserrat et al. 1991, 1998, 2006). Satellite and radar products were found to be useful for detecting some processes, such as precipitation bands and IGWs; nevertheless, the processes observed at the level of cloud-tops are not always manifested at the sea surface, as found in this study for some IGWs; and manifestation of the atmospheric disturbance at the sea surface is a requirement for the generation of destructive meteotsunamis.

A comparison of the radar reflectivity images with satellite images brings a certain level of discrepancy because the radar data depicted a broad region of rather high reflectivity values, which point to at least some convection within the cloud band, whereas satellite-measured brightness temperatures suggest that the frontal cloud band consists of clouds

with warm cloud-tops (cloud-top temperatures not lower than 230 °K). One should, however, keep in mind that the nature of radar and satellite measurements is very different; satellite measures radiance that is related to the temperature of the radiating cloud particles, with a spatial resolution of 4 × 4 km in sub-satellite point, whereas radar actually 'sees' the raindrops or cloud droplets with incomparably higher resolution.

Furthermore, this case might also be the one where convection is in place, but the cloud-tops are not very cold. Such cases have been observed, for example, over Europe in the Meteosat Second Generation data (Valachova et al. 2011). The reason that convective clouds have warm tops is due to the lowering of the tropopause, which in the case of the cold front causing the Boothbay event was evident from the radiosounding data. Until 00:00 UTC on 29 October, the tropopause lowered to 450 hPa (approximately 6 km), as observed in Fig. 8b. The lowering of tropopause presumably prevented an occurrence of deep convection processes; if so, the environment for occurrence of wave-CISK mechanism was not at place as found during some meteotsunami events (Belušić et al. 2007).

Numerical model simulation showed that the IGWs of wavelengths similar to wavelengths observed by radar imagery and propagating towards the shore were presumably the generator of the shallow ocean waves. Some of them reached the sea surface and were modelled to be capped by instability and ducted towards the coast, causing rates of ground air-pressure change up to 2.5 hPa/3 min. These tendencies were sufficiently high to generate long ocean waves over several tens of kilometres, thus being favourable for the Proudman resonance to occur, e.g., the meteotsunami decision matrix for the central Adriatic had a threshold of 2.5 hPa/5 min for the potential occurrence of a destructive meteotsunami (Šepić and Vilibić 2011). Additionally, the IGWs were found to be persistent and weakly dispersive, which is also a compulsory characteristic of IGWs found during meteotsunamis. Furthermore, spatially smaller and more energetic air-pressure wave packets are more efficient in energy transfer towards the sea than wider disturbances (Vilibić 2008). It should be, however, emphasized that performing successful numerical simulations of non-dispersive IGWs of wavelengths close to 10 km is quite challenging. First, in numerical models, fully non-dispersive wave packets cannot be maintained due to the inherent numerical diffusion that secures the numerical stability of the model. Therefore, the simulated wave packet in the simulation is always weakly dispersive, which should be taken into account when comparing simulation results with theories. Second, the wavelength of these pressure oscillations is close to the 10 grid spacings of the mesoscale model setup used for this study. Typically, the numerical diffusion in the WRF mesoscale model, on average, reduces the effective model resolution to 6–7 grid spacings (Skamarock 2004). However, IGWs in numerical models could be numerically diffused even for higher wavelength-grid spacing ratios, which at certain conditions might be greater than 10 (Schroeder and Schlünzen 2009). In other words, even with the wavelength-grid spacing ratio of 10, IGWs could be slightly underrepresented in the model, resulting in reducing the amplitude and rate of change of pressure oscillations. Third, maximum amplitudes and rates of air-pressure change might also be underestimated due to archiving of the modelled data every 3 min. Therefore, it is very likely that numerical modelling at sub-kilometre grid spacing resolutions (e.g., Horvath et al. 2012) and storing data at a 1-min interval comprise a preferred numerical setup when simulating IGWs potentially related to meteotsunamis.

Furthermore, the simulation of the exact location and intensity of individual convective cells in the precipitation band is near the limits of mesoscale models and the initial and boundary conditions provided by the global models. The somewhat inaccurate simulation of individual convective cells near the rear end of the precipitation band may affect the

exact location and properties of the related IGWs. Additionally, this inaccuracy also limited the analysis of the role of individual convective cells in this event. Since the precipitation band with embedded convective cells moved over the area, the effect of convection and/or a wave-CISK mechanism may appeal as possible mechanisms for inducing surface pressure oscillations or maintenance of IGWs. However, this scenario appears less likely in this event because (1) the event occurred near the rear edge of the precipitation band where around the time of meteotsunami there was no deep convection in the Boothbay area (as discussed earlier reflectivity values over the area from 18:30 UTC to 19:00 UTC were below 30 dBZ) and (2) in the simulated convective precipitation band, the lines of the maximal vertical velocity did not slope with the height, such as required in the wave-CISK model. However, due to uncertainties related to insufficient observational data and limits of mesoscale simulation accuracy, the possibility of a pressure perturbation of convective origin cannot be completely discarded as a concomitant factor in the Boothbay event.

Finally, the creation of an early meteotsunami warning system is still difficult to achieve, at least using the observing systems that are presently available in the Gulf of Maine. In addition to the obligatory higher sampling rates that should be applied to the meteo and ocean measurements, the network should be spatially dense enough to capture the characteristics of an atmospheric disturbance found to be important for generation of destructive meteotsunamis: intensity, speed, direction and dispersiveness. The measurements should be over the sea, which makes the meteotsunami observing and warning network rather expensive. In addition, an early warning system based on meteo and ocean observations will only be able to raise an alarm an hour or so before arrival of the waves to the shore, as the generation of destructive meteotsunami waves through open-ocean resonance normally occurs over a few hours or less (Monserrat et al. 2006). Other approaches include an assessment of the synoptic conditions that may be similar during meteotsunami events recorded at a single area; namely, the Balearic meteotsunamis or *rissagas* occur during specific synoptic conditions that are favourable for the generation of IGWs and other energetic propagating disturbances, which are used for qualitative forecasting of the phenomenon (Jansà et al. 2007). Furthermore, the analysis of 16 north Adriatic meteotsunami episodes revealed that they as well occur under very specific synoptic conditions, which may be useful for qualitative meteotsunami forecasts (Šepić et al. 2012). This approach demands long-term measurements and a sufficient number of meteotsunami cases to be analyzed, which is not presently achievable for Boothbay Harbor; however, it allows the qualitative forecast to be issued a few days in advance. The final early warning tools are numerical models, which are presently capable of reproducing a meteotsunami, but not always accurately or as intensely as observed, while rapid execution of an ensemble of model runs and its proper assessment is still not a realistic option.

6 Conclusions

We investigated the source and physical mechanisms of the observed tsunami-like waves that hit Boothbay Harbor, Maine and neighbouring areas, frightening the coastal population and producing limited damage. Recorded data revealed rapid air-pressure and wind changes that were associated with the passage of the frontal precipitation band, precisely its rear side, where IGWs were detected by radar observations. Satellite and radar observations also revealed a train of convective cells approaching the area around the time of the event, but no deep convection occurred near the Boothbay area. Numerical modelling

reproduced the IGWs that occurred over the Gulf of Maine and propagated towards the coast with speeds of approximately 28–30 ms^{-1}. Numerical modelling exhibited a vertical structure favourable for trapping of the IGWs in the lower troposphere. At the surface, IGWs manifested as pronounced and rapid air-pressure oscillations. Additionally, the environment was conducive to long-distance maintenance of the IGWs over the Gulf of Maine area, allowing for the resonant transfer of energy towards the ocean. It is reasonable to assume, as found during worldwide meteotsunami cases, that generated ocean waves travelled together with ground atmospheric disturbances and the IGWs towards the coast and were amplified through resonance along its pathway and finally strongly intensified within harbours and bays of high amplification factors. However, the generation of meteotsunami waves will be a part of future studies, together with a numerical assessment of the meteotsunami wave heights when different atmospheric disturbance parameters are imposed (speed, direction, shape, intensity) to the sea.

The present observation systems were found to be inadequate for capturing the disturbance; both sampling resolution and spatial density were found to be insufficient. Numerical models successfully explained the physics of the presumed meteotsunami source in the atmosphere; however, their use as an eventual early warning systems still demand extensive research to better reach quantitative performance, as meteotsunamis are a multiresonant phenomenon where a small change in force may result in a significant reduction or amplification of the destructiveness of an event. However, a timely and reliable forecast with multiparameter threshold-exceeding protocols, similar to a tsunami decision matrix, could significantly increase the preparedness of endangered population and reduce the possible economical losses.

References

Belušić D, Strelec-Mahović N (2009) Detecting and following atmospheric disturbances with a potential to generate meteotsunamis in the Adriatic. Phys Chem Earth 34:918–927

Belušić D, Grisogono B, Klaić ZB (2007) Atmospheric origin of the devastating coupled air-sea event in the east Adriatic. J Geophys Res 112:D17111. doi:10.1029/2006JD008204

Chen F, Dudhia J (2001) Coupling an advanced land surface-hydrology model with the Penn State-NCAR MM5 modeling system. Part I: model implementation and sensitivity. Mon Wea Rev 129:569–585

Cheng CM, Alpers W (2010) Investigation of trapped atmospheric gravity waves over the South China Sea using Envisat Synthetic Aperture Radar images. Int J Remote Sens 31:4725–4742

Churchill DD, Houston SH, Bond NA (1995) The Daytona Beach wave of 3–4 July 1992: a shallow water gravity wave forced by a propagating squall line. Bull Am Meteorol Soc 76:21–32

De Jong MPC, Battjes JA (2004) Low-frequency sea waves generated by atmospheric convection cells. J Geophys Res 109:C01011. doi:10.1029/2003JC001931

Dragani WC, Mazio CA, Nuñez MN (2002) Sea level oscillations in coastal waters of the Buenos Aires province, Argentina. Cont Shelf Res 22:779–790

Dudhia J (1989) Numerical study of convection observed during the winter monsoon experiment using a mesoscale two-dimensional model. J Atmos Sci 46:3077–3107

Ek MB, Mitchell KE, Lin Y, Rogers E, Grunmann P, Koren V, Gayno G, Tarpley JD (2003) Implementation of Noah land surface model advances in the National Centers for Environmental Prediction operational mesoscale Eta model. J Geophys Res 108(D22):8851. doi:10.1029/2002JD003296

Haslett SK, Bryant EA (2009) Meteorological tsunami in Southern Britain: an historical review. Geogr Rev 99:146–163

Hibiya T, Kajiura K (1982) Origin of the Abiki phenomenon (a kind of seiche) in Nagasaki Bay. J Oceanogr Soc Jpn 38:172–182

Horvath K, Koracin D, Vellore RK, Jiang J, Belu R (2012) Sub-kilometer dynamical downscaling of near-surface winds in complex terrain using WRF and MM5 mesoscale models. J Geophys Res 117:D11. doi:10.1029/2012JD017432

Janjić ZI (1996) The surface layer in the NCEP Eta model. 11th conference on NWP, Norfolk, VA, Am Meteorol Soc, pp 354–355

Janjić ZI (2001) Nonsingular implementation of the Mellor-Yamada Level 2.5 scheme in the NCEP meso model. NCEP Office Note No. 437, 61 pp

Jansà A, Monserrat S, Gomis D (2007) The rissaga of 15 June 2006 in Ciutadella (Menorca), a meteorological tsunami. Adv Geosci 12:1–4

Kain JS (2004) The Kain-Fritsch convective parameterization: an update. J Appl Meteorol 43:170–181

Kain JS, Fritsch JM (1993) Convective parameterization for mesoscale models: The Kain-Fritsch scheme. In: Emanuel KA, Raymond DJ (eds) The representation of cumulus convection in numerical models. Am Meteorol Soc, Boston, pp 165–170

Kidder SQ, Vonder Haar TH (1995) Satellite meteorology: an introduction. Academic Press, San Diego, p 466

Laprise R (1992) The Euler equations of motion with hydrostatic-pressure as an independent variable. Mon Wea Rev 120:197–208

Lin Y-L (2007) Mesoscale dynamics. Cambridge University Press, Cambridge, p 630

Lindzen RS (1974) Wave-CISK in the tropics. J Atmos Sci 31:156–179

Lindzen RS, Tung K–K (1976) Banded convective activity and ducted gravity waves. Mon Wea Rev 104:1602–1617

Mecking JV, Fogarty CT, Greatbatch RJ, Sheng J, Mercer D (2000) Using atmospheric model output to simulate the meteorological tsunami response to Tropical Storm Helene (2000). J Geophys Res 114:C10005. doi:10.1029/2009JC005290

Mellor GL, Yamada T (1974) Hierarchy of turbulent closure models for planetary boundary-layers. J Atmos Sci 31:1791–1806

Mellor GL, Yamada T (1982) Development of a turbulent closure-model for geophysical fluid problems. Rev Geophys 20:851–875

Mercer D, Sheng J, Greatbatch RJ, Bobanović J (2002) Barotropic waves generated by storms moving rapidly over shallow water. J Geophys Res 107(C10):3152. doi:10.1029/2001JC001140

Mlawer EJ, Taubman SJ, Brown PD, Iacono MJ, Clough SA (1997) Radiative transfer for inhomogeneous atmospheres: RRTM, a validated correlated-k model for the longwave. J Geophys Res 102: 16663–16682. doi:10.1029/97JD00237

Monserrat S, Thorpe AJ (1992) Gravity-wave observation using an array of microbarographs in the Balearic Islands. Q J R Meteorol Soc 118:259–282

Monserrat S, Thorpe AJ (1996) Use of ducting theory in an observed case of gravity waves. J Atmos Sci 53:1724–1736

Monserrat S, Ramis C, Thorpe AJ (1991) Large-amplitude pressure oscillations in the Western Mediterranean. Geophys Res Lett 18:183–186

Monserrat S, Rabinovich AB, Casas B (1998) On the reconstruction of the transfer function for atmospherically generated seiches. Geophys Res Lett 25:2197–2200

Monserrat S, Vilibić I, Rabinovich AB (2006) Meteotsunamis: atmospherically induced destructive ocean waves in the tsunami frequency band. Nat Hazards Earth Syst Sci 6:1035–1051

Nappo CJ (2002) An Introduction to Atmospheric Gravity Waves. Academic Press, San Diego, p 276

Nikolkina I, Didenkulova I (2012) Catalogue of rogue waves reported in media in 2006-2010. Nat Hazards 61:989–1006

Orlić M, Belušić D, Janeković I, Pasarić M (2010) Fresh evidence relating the great Adriatic surge of 21 June 1978 to mesoscale atmospheric forcing. J Geophys Res 115:C06011. doi:10.1029/2009JC005777

Pawlowicz R, Beardsley B, Lentz S (2002) Classical tidal harmonic analysis including error estimates in MATLAB using T_TIDE. Comput Geosci 28:929–937

Paxton CH, Sobien DA (1998) Resonant interaction between an atmospheric gravity wave and shallow water wave along Florida's west coast. Bull Am Meteorol Soc 79:2727–2732

Proudman J (1929) The effects on the sea of changes in atmospheric pressure. Geophys Suppl Mon Notices R Astron Soc 2(4):197–209

Rabinovich AB (2009) Seiches and harbour oscillations. In: Kim YC (ed) Handbook of Coastal and Ocean Engineering. World Scientific Publ, Singapore, pp 193–236

Reisner J, Rasmussen RM, Bruintjes RT (1998) Explicit forecasting of supercooled liquid water in winter storms using the MM5 mesoscale model. Q J R Meteor Soc 124B:1071–1107

Renault L, Vizoso G, Jansá A, Wilkin J, Tintoré J (2011) Toward the predictability of meteotsunamis in the Balearic Sea using regional nested atmosphere and ocean models. Geophys Res Lett 38:L10601. doi:10.1029/2011GL047361

Sallenger AH Jr, List JH, Gelfenbaum G, Stumpf RP, Hansen M (1995) Large wave at Daytona Beach, Florida, explained as a squall-line surge. J Coastal Res 11:1383–1388

Schroeder G, Schlünzen KH (2009) Numerical dispersion of gravity waves. Mon Wea Rev 137:4344–4354

Šepić J, Vilibić I (2011) The development and implementation of a real-time meteotsunami warning network for the Adriatic Sea. Nat Hazards Earth Syst Sci 11:83–91

Šepić J, Vilibić I, Belušić D (2009) The source of the 2007 Ist meteotsunami (Adriatic Sea). J Geophys Res 114:C03016. doi:10.1029/2008JC005092

Šepić J, Vilibić I, Strelec Mahović N (2012) Northern Adriatic meteorological tsunamis: observations, link to the atmosphere, and predictability. J Geophys Res 117:C02002. doi:10.1029/2011JC007608

Skamarock WC (2004) Evaluating mesoscale NWP models using kinetic energy spectra. Mon Wea Rev 132:3019–3032

Skamarock WC, Klemp JB (2008) A time-split nonhydrostatic atmospheric model for weather research and forecasting applications. J Comput Phys 227:3465–3485

Tanaka K (2010) Atmospheric pressure-wave bands around a cold front resulted in a meteotsunami in the East China Sea in February 2009. Nat Hazards Earth Syst Sci 10:2599–2610

Thomson RE, Rabinovich AB, Krassovski MV (2007) Double jeopardy: concurrent arrival of the 2004 Sumatra tsunami and storm-generated waves on the Atlantic coast of the United States and Canada. Geophys Res Lett 34:L15607. doi:10.1029/2007GL030685

Thomson RE, Rabinovich AB, Fine IV, Sinnott DC, McCarthy A, Sutherland NAS, Neil LK (2009) Meteorological tsunamis on the coasts of British Columbia and Washington. Phys Chem Earth 34:971–988

Valachova M, Pucik T, Zak M (2011) Severe convective weather of the 15th August 2010. WDS'11 proceedings of contributed papers, part III, pp 72–77

Vilibić I (2008) Numerical simulations of the Proudman resonance. Cont Shelf Res 28:574–581

Vilibić I, Šepić J (2009) Destructive meteotsunamis along the eastern Adriatic coast: overview. Phys Chem Earth 34:904–917

Vilibić I, Domijan N, Orlić M, Leder N, Pasarić M (2004) Resonant coupling of a traveling air pressure disturbance with the east Adriatic coastal waters. J Geophys Res 109:C10001. doi:10.1029/2004JC002279

Vilibić I, Šepić J, Ranguelov B, Strelec Mahović N, Tinti S (2010) Possible atmospheric origin of the 7 May 2007 western Black Sea shelf tsunami event. J Geophys Res 115:C07006. doi:10.1029/2009JC005904

Yankovsky AE (2009) Large-scale edge waves generated by hurricane landfall. J Geophys Res 114:C03014. doi:10.1029/2008JC005113